Materials for Renewable and Sustainable Energy (2024) 13:69–79
https://doi.org/10.1007/s40243-023-00251-6

ORIGINAL PAPER

Significant augmentation of proton conductivity in low sulfonated polyether sulfone octyl sulfonamide membranes through the incorporation of hectorite clay

Walid Mabrouk[1] · Khaled Charradi[2] · Imen Ben Kacem[1,3] · Ridha Lafi[1] · Nizar Bellakhal[3] · Riadh Marzouki[4] · Sherif M. A. S. Keshk[5]

Received: 7 October 2023 / Accepted: 13 December 2023 / Published online: 16 February 2024

Abstract
An innovative methodology was employed to fabricate ion exchange membranes tailored for fuel cell applications. This approach entailed blending low sulfonated polyether sulfone octyl sulfonamide (LSPSO) with Hectorite (Hect) clay at varying weight percentages (1 wt%, 3 wt%, and 6 wt%). The resultant composite membranes underwent comprehensive characterization via Fourier transform infrared spectroscopy, X-ray diffraction, scanning electron microscopy, and thermogravimetric analysis, aiming to assess their surface morphology and thermal resilience. Remarkably, the thermal stability of the composite membrane exhibited a substantial enhancement in comparison to the pristine LSPSO membrane. Moreover, the incorporation of 6 wt% Hectorite into the composite membrane yielded a noteworthy amplification in proton conductivity, achieving a fourfold increase (141.66 mS/cm) as opposed to the LSPSO membrane in isolation (35.04 mS/cm). Consequently, the Hect/LSPSO composite membrane exhibits remarkable potential as an electrolyte membrane for fuel cells operating at temperatures surpassing 100 °C.

Keywords Composite membrane · Proton conductivity · LSPSO · Hectorite clay

Introduction

Extensive research has been conducted to study the use of ion-exchange membranes in proton-exchange membrane fuel Cells (PEMFCs). The proton-exchange membrane (PEM), a crucial component of any direct methanol fuel cells (DMFCs), serves as a barrier between the anode and cathode reactants while still allowing protons to pass between the electrodes when the cell is in operation. Aromatic polymers are particularly well-suited for such applications due to their favorable combination of high heat stability and simplicity of handling [1]. The aromatic ring is typically a top choice for modification, resulting in the production of polymers with better properties.

Specifically, sulfonated polyether sulfone (SPES) has exhibited numerous improvements to be used as a solid electrolyte for PEMFC [2]. Investigations have likewise been done in the use of polyether sulfone (PES) in diverse domains such as proton exchange membrane fuel cell [2], electrodialysis [3], modified electrode [4], super-capacitors [5], and direct methanol fuel cells (DMFC) [6]. DMFCs, identified as a distinct class of energy converters, demonstrate ideal compatibility for use in mobile electronic gadgets and transport applications because of their enhanced energy storage capacity at comparatively cooler temperatures, along with the convenience of managing a fluid energy substrate [7]. The significant technical challenges stem from the slow methanol oxidation rates and the pronounced migration of

✉ Walid Mabrouk
w.mabroukcerte@gmail.com

1 Laboratory Water, Membrane and Biotechnology of the Environment, Technoparc Borje Cedria, CERTE, BP 273, 8020 Soliman, Tunisia

2 Nanomaterials and Systems for Renewable Energy Laboratory, Research and Technology Center of Energy, Technoparc Borje CedriaCRTEn, BP 095 Hammam Lif, Tunisia

3 Ecochimie Laboratory, National Institute of Applied Sciences and Technology, University of Carthage, Tunis, Tunisia

4 Department of Chemistry, Faculty of Science and Arts, King Khalid University, Abha, Saudi Arabia

5 Become: Deep Tech & Nanoscience, 63 Rue de Tolbiac, 75013 Paris, France

methanol from the anode side to the cathode side [8]. Commercial progress in DMFCs encounters significant hurdles, primarily marked by reduced energy utilization and inferior unit functionality because of extensive methanol passage through Nafion membranes. The polymer ion-conductive layer, which aids in moving protons between the anode and cathode and effectively separates anode (methanol) and cathode (oxygen) reactants, determines the degree of methanol crossover [9]. Recent research emphasis on ion-conductive layers suitable for DMFCs and ion-conductive layer (PEM) energy units has been on the evolution of sulfonated polyether sulfone octyl sulfonamide (SPESOS)-type layers. However, current versions of these membranes do not fully satisfy strict criteria for real-world DMFC uses. The significant impediment to achieving DMFC viability in real-world scenarios primarily stems from the high methanol permeation rate across the membrane. Like the electro-osmotic drag observed in aqueous systems, methanol exhibits a protonic drag phenomenon [10]. Sulfonated polyether sulfone (SPES) has showcased several enhancements that render it suitable for deployment as a robust solid electrolyte within the context of PEMFCs [10]. Moreover, studies exploring the use of PES concerning direct methanol fuel cells (DMFCs) have taken place.

In these investigations, PES was combined with sulfonated polyether variants or sulfonated polymeric sulfones to create polymer mixtures, which were then synthesized and thoroughly characterized [10]. The attractive features of SPES meet all the necessary criteria to be used within a perfect PEMFC. However, this material exhibits specific constraints because of the inherent mechanical characteristics of this polymer type. Various versions of sulfonated polyether sulfone octyl sulfonamide (SPESOS) arise by integrating different amounts of octylamine into the SPES structure. Since SPESOS is not water-soluble, the resulting membranes show structural vulnerabilities and present a broad range in ion transport and moisture uptake, depending on how much octylamine is integrated. Several techniques were proposed for improving both the ion transport properties and structural features in these layers. Several studies have been conducted on blending unmodified PES with various sulfonated hydrocarbon polymers to have significant ionic conductivity. PES is utilized as an inert hydrophobic polymer in all these scenarios to alter the microstructure of the resultant membrane. Although the technique lowers swelling and methanol crossover, it has an undesirable influence on the proton conductivity of the resultant electrolyte and consequently on the overall performance of the device [11]. On the other hand, the forefront of materials innovation has seen the emergence of polymer/clay composites, which serve as reinforcements in well-structured polymers as well as conventional micro- and macro-composite polymers. These polymer composites boast a range of desirable properties, including heightened elastic modulus, and enhanced the water uptake of the composite membranes with increasing clay content owing to an increase in hydrophilicity [12, 13]. The incorporation of clays onto polymer decreases the energy of activation (Ea) and prevents electric field erosion with improvement in the corona resistance of composite membranes. However, the proton conductivity of SPESOS was enhanced via the incorporation of sepiolite clay (at 1%, 3%, and 6% by weight) [11].

Compared to the pristine SPESOS, the sepiolite nanostructured substance showed enhanced properties concerning moisture holding, surface interaction, and ion transport. These findings suggest composite layers demonstrated improved water-attracting properties with an elevated capacity for ion exchange compared to untouched SPESOS [12]. Montmorillonite (MMT)/SPESOS composite membranes were meticulously crafted, subjected to comprehensive analysis, and evaluated for their viability as electrolytic membranes within the realm of fuel cell applications. Among these combinations, the SPESOS/MMT composite containing 1% MMT by weight demonstrated peak performance, signifying its potential as a highly promising composite material for utilization in electrochemical applications [12]. Hectorite is an indigenous stratified mineral composed of magnesium, lithium, and silicate elements. Classified as a trioctahedral clay mineral within the smectite group, its theoretical chemical composition conforms to $Na_{0.3}Mg_{2.7}Li_{0.3}Si_4O_{10}(OH)_2$ [13]. Hectorite displays a layered structure defined by Si-O-Mg (Li)-O-Si sequences, and between these sequences, there are spaces containing water-associated ions such as Na^+ and Li^+. Each layer consists of a Mg-O-Li octahedral layer flanked by a pair of Si-O-Si tetrahedral layers, leading to an estimated thickness of 0.96 nm [14]. What sets Hectorite clay apart from other varieties is its substantial, negatively charged, plate-like structure. This structure features exchangeable counter cations sandwiched between delicate platelets, which are approximately 1 nm in thickness and possess a diameter of approximately 250 nm [15]. Compared with the restricted movement of large clay ion fragments, proton movement shows significant prominence. Within the context of LSPSO, the inclusion of Hectorite clay serves as a bridge to the ionic clusters, fostering the restoration of hydrophilic properties as an outcome.

In this perspective, the purpose of the present work was to synthesize a novel kind of composite with the low-sulfonated polyether sulfone octyl sulfonamide (LSPSO) matrix incorporating Hectorite clay to enhance moisture retention and ion transport capacities inside the LSPSO layers. To achieve this goal, various Hectorite clay loading ratios were employed in the fabrication of Hectorite/LSPSO composite membranes, which were subsequently subjected to structural and morphological assessments. The development of a proton-conductive polymer composite will involve a

comprehensive examination of its thermal stability, water retention capacity, and proton conductivity. This innovative composite has potential use in multiple areas, encompassing areas like electric chemical detectors, heat transmitters, and associated domains.

Experimental

Resources

The clay employed in this study originated from a natural source in Tunisia, specifically Hectorite, with the following chemical composition: $H_2LiMgNaO_{12}Si_4{}^{-2}$. Moreover, the low-sulfonated polyether sulfone octyl sulfonamide (LSPSO) used for the study was produced by the Eras Labo company [10, 16]. Sulfuric acid along with sodium hydroxide came from Scharlau and Laurylab, respectively, whereas the solvent *N*,*N*´-dimethylacetamide (DMAc) was sourced from Acros.

Membrane preparation

The methodology outlined earlier was employed for the synthesis of the low-sulfonated polyether sulfone octyl sulfonamide compound, denoted as LSPSO [10]. The Hectorite/LSPSO composite membrane was created using the produced LSPSO having a sulfonation level equivalent to a single proton for each molecular unit (CEI = 1.8 meq/g). Following a 15-min stirring period, a casting solution was formulated, comprising LSPSO (10 wt%) evenly dispersed in 10 mL of DMAc, yielding a homogeneous and transparent solution. A 10 wt% LSPSO solution was blended with Hectorite clay in varying weight ratios (1%, 3%, and 6%), and composite membranes were generated through the casting evaporation technique. Subsequently, the produced membranes underwent drying at 80 ºC. Notably, all the membranes exhibited a consistent thickness of approximately 100 µm.

Membrane characterization

The study utilized Fourier Transform Infrared (FT-IR) examination with an IR200 FT-IR spectrophotometer from Nicolet in the transmission mode. Spectral information for LSPSO along with different composite layers was gathered between 400 and 4000 cm^{-1} [17]. For spectral examination, sample layers were placed amid cast iron and diamond crystal (serving as a dividing blade) bypassing the pre-processing stages. This methodology was employed to ensure a meticulous examination of the membrane's attributes and to facilitate the investigation of its constituent functional groups.

X-ray diffraction analysis was conducted using the automated Bruker D8 Advance system. Diffractograms of the desiccated composite membrane specimens were acquired within the angular range spanning from 5 to 60 degrees (2 θ) [18]. No preparatory treatments were administered to the specimens prior to analysis. The X-ray diffraction examination facilitated an evaluation of the crystalline structure of LSPSO and its composite counterparts. To determine the measurements of crystalline structures, the Scherrer formula was utilized:

$$D = (\kappa\lambda/\beta \mathrm{D}\ \mathrm{COS}\theta). \tag{1}$$

Here, D stands for the size of crystalline structures in nm, λ indicates radiation's length (1.54056 Å for CuKα radiation), κ remains a consistent figure at 0.94, βD points to the breadth of the peak at its half-maximum strength, and θ relates to where the peak is located. This assessment yielded valuable insights into the structural attributes of the materials under scrutiny.

Thermogravimetric analysis (TGA) was conducted utilizing a Mettle TGA instrument. Before the examination, membrane samples with weights around 2.5 and 3.5 mg underwent a drying phase for 24 h at 100 °C to remove remaining wetness and solvent elements [19]. Afterward, the TGA software was set up to progressively increase the temperature starting at 25 °C and ending at 900 °C, with a temperature rise pace of 10 °C every minute. A consistent nitrogen stream, moving at 40 mL every minute, was maintained throughout the entire examination. This TGA protocol facilitated the evaluation of the thermal resilience and degradation patterns of the membrane specimens over an extensive temperature spectrum.

For assessing membranes' moisture absorption (WU), dry specimens were utilized. Assessments of moisture absorption took place by immersing every membrane in purified water at room temperature over a 72-h span. After soaking, excess water on the surface was gently removed with absorbent paper, and then the damp mass for each membrane was recorded. WU figures were then determined by calculating the relative weight gain for each initial dehydrated sample [20]. Calculation entailed taking the difference between the mass of the initial dehydrated sample and the mass post-water absorption. Equation (2) was employed to derive the WU values.

$$WU = \frac{W_{\mathrm{wet}} - W_{\mathrm{dry}}}{W_{\mathrm{dry}}} * 100. \tag{2}$$

Within this scenario, W_{wet} and W_{dry} denote the weights for moistened and dried layers, in that order.

For different layers, the angle of contact (CA) was evaluated using a Theta visual tension measuring device. A 5 µL droplet from purified water was carefully placed on each

layer's surface, and an image showcasing the droplet was taken using a photographic device [21]. Afterward, the angle of contact was determined using a dedicated digital tool, Theta, which analyzed the taken droplet picture and measured the angle created between the droplet and the layer's surface.

To study the surface texture and cross-sectional architecture of the layer, scanning electron microscopy (SEM) was utilized with tools from Carl-Zeiss AG, Germany. The membranes were meticulously fractured under controlled conditions, with cooling achieved through liquid nitrogen, to enable comprehensive analysis [22].

Assessing the ionic exchange capability (IEC) took place via base and acid evaluation. Every single ion transfer layer, with dimensions of 5×5 cm^2, was submerged in a NaOH solution (100 mL, 10^{-2} M) for two days. This procedure facilitated the conversion of sulfonated groups (SO_3H) within the membranes into sodium groups (SO_3Na) via an ion exchange mechanism. As a result, protons released from sulfonated clusters within the mixture were effectively balanced out with hydroxide ions, producing H_2O. For IEC calculation, both the starting mixture and NaOH blend were titrated using water-based sulfonic acid solutions. The volume of sulfonic acid required to reach the titration endpoint was then employed to deduce the concentration of the sodium hydroxide solution that had reacted with the sulfonated groups in the membrane [23]. Ultimately, the individual IEC for each membrane was ascertained by employing the subsequent formula:

$$\mathrm{IEC} = \frac{n^{i}_{\mathrm{NaOH}} - n^{f}_{\mathrm{NaOH}}}{W_{\mathrm{dry}}}. \tag{3}$$

In this context, n^{i}_{NaOH} stands for the starting molar amount of NaOH in the mixture (10^{-2} M, 200 mL), n^{f}_{NaOH} indicates the molar amount of NaOH post-exchange, and Wdry points to the weight of the dried layer.

For assessing the ion transport capability in the layers, EIS techniques were utilized with a Biologic Science Instruments VSP potentiostat. The experimental configuration entailed varying both temperature and the amount of Hectorite additive to assess their respective effects on proton conductivity. Electrical resistance (R) for each layer was determined through identifying the intersection point between high-frequency Nyquist diagrams and the x-axis [24, 25]. Ionic conductance (σ), measured in mS/cm, was determined using the following formula:

$$\sigma(\mathrm{mS/cm}) = \frac{e}{R \times S}. \tag{4}$$

This formula served as a quantitative means to assess the ionic conductivity of the membranes, leveraging the data acquired from EIS measurements. Within this context, 'e' signifies the width, 'S' stands for the membrane's surface area situated between the pair of electrodes, and 'R' denotes the electrical opposition.

Results and discussion

Fourier transform infrared spectroscopy

The uniform distribution of both organic and inorganic constituents was evident in the composite membranes, which exhibited a substantial thickness, translucence, and a pale, light-grayish-white appearance. Given the limited clay content within the composites, the spectral profiles of the diverse composite membranes exhibit a noticeable degree of similarity. Figure 1 illustrates the FT-IR spectra of the pristine LSPSO as well as those of the composite membranes for reference.

In the hybrid layers, the distinct LSPSO peaks related to the asymmetric and symmetric vibrations of O = S = O at 1020 and 1086 cm^{-1}, as well as the carbon bands at 1482 and 1583 cm^{-1}, displayed a decrease in intensity [16]. These findings illustrate the occurrence of noncovalent interactions between the LSPSO chains and the basal planes of the Hectorite. Precisely, the movement of these two peaks towards lower wavenumbers indicates the formation of non-covalent connections, suggesting the presence of hydrogen bonding between LSPSO and Hectorite clay while creating the composite. Unfortunately, because of the interference caused by the Si-O-Si absorbance band with the LSPSO bands in this specific scenario, a noticeable shift in the Si-O-Si absorbance band was not observable.

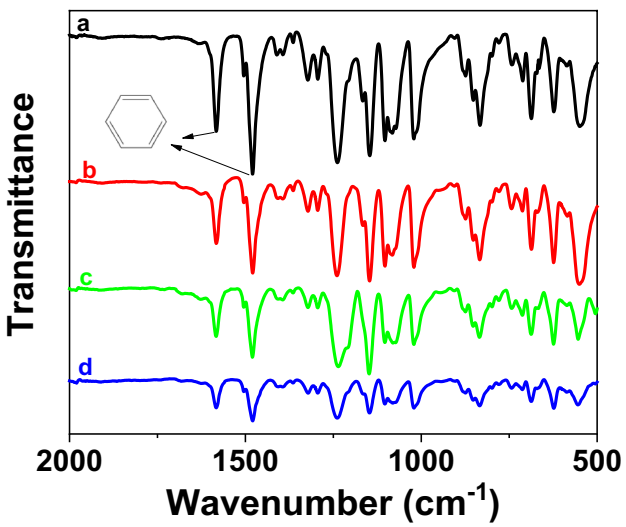

Fig. 1 FT-IR spectra. **a** LSPSO, **b** 1 wt% Hect/LSPSO, **c** 3 wt% Hect/LSPSO and **d** 6 wt Hect/LSPSO

X-ray diffractograms

Figure 2 displays the data derived from XRD diffractograms, revealing the crystal arrangements in LSPSO and the combined layers.

LSPSO, located at approximately 2θ = 14.0° and 18.0º, corresponds to the 001 and 110 planes of LSPSO. Upon the amalgamation of Hectorite into the LSPSO matrix, there was a rise in the strength of the diffraction peak related to the 001 and 110 planes of LSPSO, running perpendicular to the hybrid's surface. Additionally, the diffraction peaks of the hybrid shifted towards lower angles because of the clay's presence, leading to an enlargement of the d-spacing in the low-angle region, as elaborated in Table 1. Furthermore, the major characteristic peak of Hectorite appeared at 2 Θ = 26.5 in diffractograms of composite owing to the presence of sodium ion that confirmed the presence of clay (Fig. 2).

The presence of clay, which possesses a smaller ionic radius compared to LSPSO, contributes to an augmentation in compressive stress, thereby modifying the lattice characteristics of the LSPSO matrix through the stacking of clay-infused LSPSO. Additionally, there is a significant increase in the crystallite size within the composite material as opposed to LSPSO, as evidenced in Table 1. This phenomenon can be attributed to disparities in atomic radii and alterations in lattice parameters at the nanometer scale, resulting from heightened surface forces stemming from the inclusion of clay.

Scanning electron microscope (SEM)

The micrographs depicted in Fig. 3 offer compelling evidence that supports the interpretation of the consistency in the composite membranes.

Significantly, the absence of visible cracks, voids, or pores serves as a validation of the robustness of the manufacturing process. It is reasonable to deduce that the introduction of Hectorite into the LSPSO membrane matrix consistently produces homogenous membranes. This uniformity can be attributed to the organization of LSPSO molecular chains into a distinct domain structure, featuring the prominent inclusion of clay nanoparticles (Hectorite), which becomes particularly apparent at a concentration of 6 mass %.

Table 1 XRD analysis of LSPSO and its composite membranes

Sample	2θ (°)	*d* (001) Å	Crystallite size
LSPSO	14.10	6.20	9.90
1 wt% Hect/LSPSO	13.36	6.61	11.37
3 wt% Hect/LSPSO	12.96	6.80	11.70
6 wt% Hect/LSPSO	12.93	6.88	13.10

Contact angle

Figure 4 depicts the application of the drop shape analysis technique to evaluate the modifications in surface characteristics of LSPSO arising from the integration of Hectorite. This approach facilitates the measurement and analysis of these alterations in surface attributes.

An effective means of assessing the super wettability of a material, particularly in composite regions, is through contact angle analysis. Through a comparison of the contact angles among various layers, we can assess the exceptional wettability of LSPSO and its associated composite materials. Pristine LSPSO layers display a contact angle measuring 87.54°. In contrast, the incorporation of Hectorite clay into the composites leads to a reduced contact angle. As illustrated in Fig. 3, the contact angles for composites incorporating 1 wt%, 3 wt%, and 6 wt% clay are recorded at 76.47°, 73.08°, and 69.71°, correspondingly.

The decline in the angle of contact signifies an improvement in water-attracting characteristics, an outcome linked to the clay's presence within the composite materials. Thus, the contact angle measurements establish that the composite membranes exhibit improved wettability compared to the individual component materials.

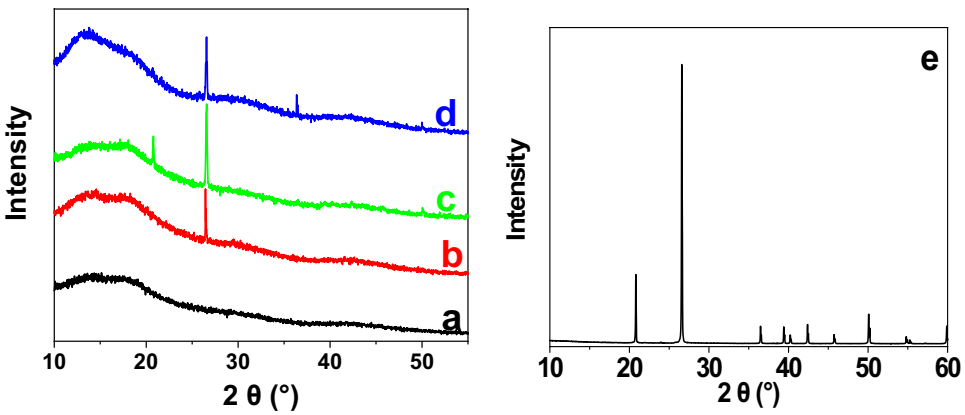

Fig. 2 X-ray diffraction patterns of **a** LSPSO, **b** 1 wt% Hect/LSPSO, **c** 3 wt% Hect/LSPSO, **d** 6 wt% Hect/LSPSO, and **e** Hectorite

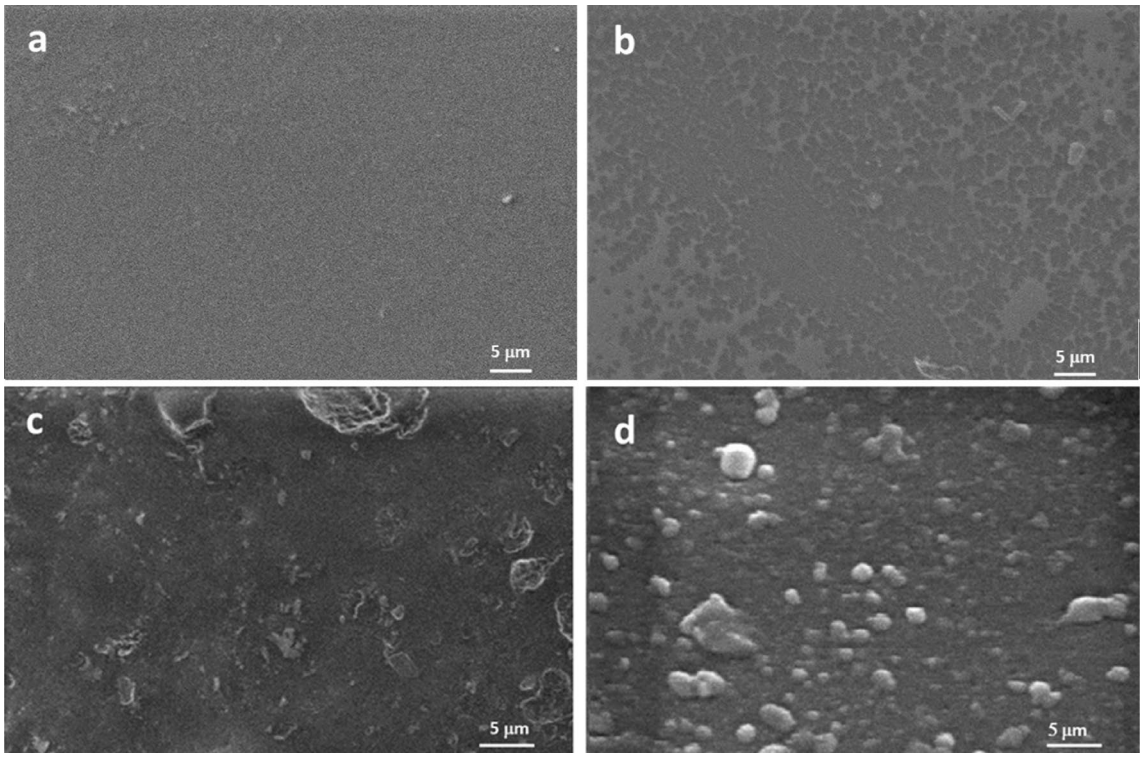

Fig. 3 SEM micrographs of surfaces membrane. **a** LSPSO, **b** 1 wt% Hect/LSPSO, **c** 3 wt% Hect/LSPSO and **d** 6 wt% Hect/LSPSO

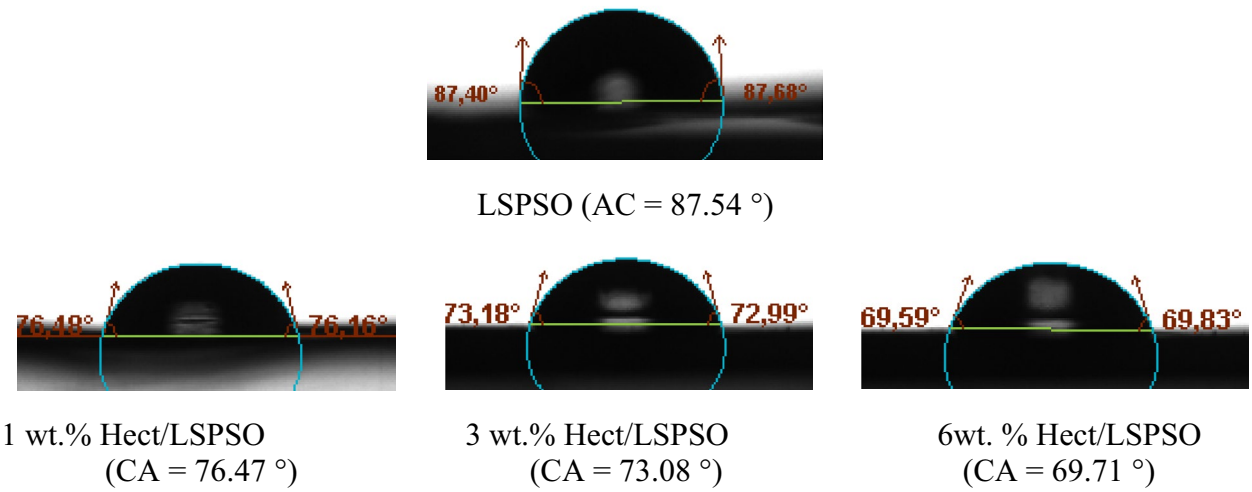

Fig. 4 Contact angle of fabricated composite membranes

Thermogravimetric analysis (TGA)

In Fig. 5, the results of the thermogravimetric analysis (TGA) for the various membranes are presented.

These findings demonstrate that the manufactured membranes exhibited consistent behavior without notable deviations or anomalies.

During thermal analysis (Fig. 5), it's noted that all layers experience three distinct phases of mass reduction. In the initial phase, taking place around 100 ºC, we can ascribe the weight loss to the evaporation of moisture from the LSPSO matrix. Following that, a noticeable decrease in mass becomes apparent at approximately 300 ºC, possibly suggesting the breakdown of sulfonic clusters (Fig. 5). Following that, there is an additional decrease in mass observed

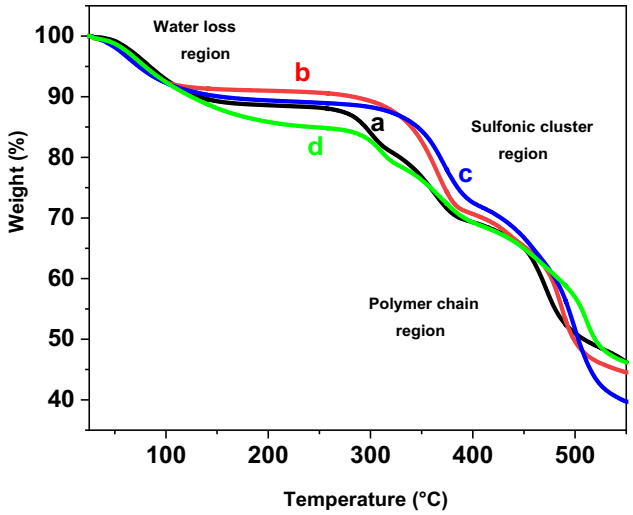

Fig. 5 Thermogravimetric analysis of **a** LSPSO, **b** 1 wt% Hect/LSPSO, **c** 3 wt% Hect/LSPSO and **d** 6 wt% Hect/LSPSO

at roughly 470 ºC, indicating the disintegration of the primary polymer structure. Upon comparing the thermogravimetric analysis (TGA) outcomes of the LSPSO membrane with those of all LSPSO composite membranes, no substantial alterations in decomposition characteristics are discernible throughout the entire temperature range examined. Nevertheless, it is noteworthy that the TGA curves of the composite membranes exhibit a tendency towards higher temperatures as Hectorite clay is incorporated into LSPSO, particularly at concentrations of 1 wt% and 3 wt%. Upon scrutinizing the TGA curves and comparing them with those of the LSPSO membrane, a comprehensive analysis reveals that the composite membranes exhibit an increased affinity for retaining water. Notably, integrating 6 wt% clay results in the most substantial moisture reduction, totaling 15%. In contrast, the combined layers with 1 wt% and 3 wt% clay exhibit moisture reductions of roughly 8 wt% and 10 wt% correspondingly. At 340°°C, the weight loss for LSPSO is around 20%, while it is less than 15% in the presence of 1 and 3 wt%. The weight loss for the pristine polymer is more than that of the composite membrane at temperatures around 400°°C, indicating that composite membranes are more stable than pristine membranes.

Ion exchange capacity

IEC measurements acquired through base and acid titration for the various membrane formulations consistently fall within the 1.8 milliequivalents per gram (meq/g) range.

The presence of neutral clay within the LSPSO matrix does not influence this measurement, affirming the compatibility of these results with the LSPSO composition. The calculation of the IEC for the LSPSO membrane involved the utilization of the average value derived from three independent measurements, yielding a value of 1.8 milliequivalents per gram (meq/g). Additionally, it was ascertained that the LSPSO material employed had a sulfonation level of 80%. Table 2 presents the documented values for both the predicted and practical ion exchange capacities of the layers, considering a 25 cm^2 surface area.

It's worth mentioning that the acquired ion exchange capacity (IEC) outcomes closely match the structure of the fabricated layers. As an example, the standard layer (LSPSO) showcases an IEC of 1.8 meq/g. Interestingly, the inclusion of nanoparticles in the composite membranes does not affect this capacity, as these nanoparticles lack sulfonation. Furthermore, a contrast between the practical and theoretical ion exchange capacity values among different layers suggests a slight difference, probably due to inaccuracies encountered in the acid–base analysis.

Water uptake

Figure 6 delineates alterations in water absorption, computed through the application of Eq. 1, in composite

Table 2 Comparison between experimental and theoretical values of ion exchange capacity of all as-prepared membranes

Membrane	Theoretical ion exchange capacity/ (meq/g)	Experimental ion exchange capacity/ (meq/g)
LSPSO	1.80	1.75
1 wt% Hect/LSPSO	1.80	1.62
3 wt% Hect/LSPSO	1.80	1.75
6 wt% Hect/LSPSO	1.80	1.79

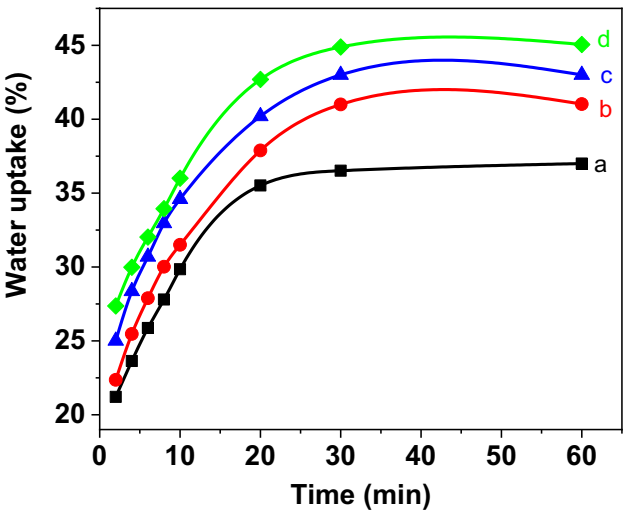

Fig. 6 Water uptake statistics of **a** LSPSO, **b** 1 wt% Hect/LSPSO, **c** 3 wt% Hect/LSPSO and **d** 6 wt% Hect/LSPSO

membranes relative to the water uptake exhibited by the LSPSO membrane (1.8 meq/g) as the percentage of Hectorite content escalates.

Figure 6 elucidates the relationship between the clay content within LSPSO membranes and composite membranes, juxtaposed with their corresponding water absorption behaviors. In contrast to unaltered LSPSO membranes, which exhibit a water uptake rate of 37%, the composite membranes demonstrate a notably enhanced capacity for water absorption. The increase in water absorption primarily results from the inherent hydrophilicity of clay, a crucial factor in enhancing water uptake, owing to the existence of sulfonic clusters within the LSPSO material. Clay has the capacity to alter the dimensions of LSPSO and induce the formation of clusters, thereby influencing the microstructure of LSPSO. The observed elevation in the rate of water absorption can be attributed to the incorporation of clay into the LSPSO matrix, leading to an expansion in aggregate volume and the development of solvated proton transport pathways. The TGA data show a consistent and progressive pattern of water absorption for the various membranes under consideration as time passes.

Within the first 2–20 min, all membranes see a quick and significant increase in water absorption. After around 20 min, the rate of water absorption stabilizes, reaching practically constant levels. When compared to the reference LSPSO membrane, membranes treated with Hectorite exhibit much higher amounts of water absorption. Following a one-hour immersion in water, water absorption ranges from 41 to 45%. Furthermore, the composite membranes have a little higher water absorption capacity than the unmodified LSPSO membrane, which has a water uptake of 37%. These data clearly imply that including Hectorite in the pristine LSPSO membrane leads to increased water absorption, a phenomenon attributed to the Hectorite nanoparticles' natural hydrophilicity. Notably, these results are exactly in line with the Thermogravimetric study results. To determine the viability of using the manufactured membrane in direct methanol fuel cell technology, the stability of these membranes in methanol must be evaluated. As a result, investigations evaluating the dimensional stability of the membranes in methanol were carried out (see Supplementary data). The results show that the membranes have insufficient stability when subjected to water–methanol mixtures, with the exception of a 25%/75% methanol/water mixture (Tables S1 and S2). This discovery raises issues, particularly in light of its anticipated employment in direct methanol fuel cells. As a result, it may be worthwhile to investigate using these membranes in fuel cell technologies that do not rely on methanol as a fuel source.

Proton conductivity

Figure 7 depicts the link between the clay content of LSPSO and composite membranes and their relative proton conductivity performances.

To evaluate the membrane's ability to facilitate proton migration and assess its electrochemical performance, AC impedance spectroscopy was employed as a diagnostic technique. The investigations were carried out over the temperature span of room temperature up to 100 °C, all the while sustaining a consistent relative humidity (RH) level of 100%, as shown in Fig. 7. Figure 7 presents a detailed analysis of the electrochemical performance of the membrane, with a specific emphasis on its ability to facilitate proton migration. The membranes exhibit a progressive enhancement in proton conduction efficiency.

In comparison to the LSPSO membrane, the modified membranes exhibit superior conductivity levels throughout the entire temperature spectrum. The results suggest that the intrinsic ionic conductivity remains reasonably consistent within the temperature span extending from 25 (room temperature) to 40 °C. Nevertheless, as the temperature exceeds 40 °C, there is a notable surge in conductivity, surpassing that of the original membrane, which stands at 35 mS/cm at 100 °C. To be precise, the composite membranes, namely 1% Hect/LSPSO, 3% Hect/LSPSO, and 6% Hect/LSPSO, exhibit conductivities in the vicinity of 112 mS/cm, 122 mS/cm, and 141 mS/cm, respectively. It is of significance to highlight that the integration of Hectorite into the LSPSO matrix leads to an augmentation in proton conductivity within the manufactured membranes. Furthermore, it is important to emphasize that the modified

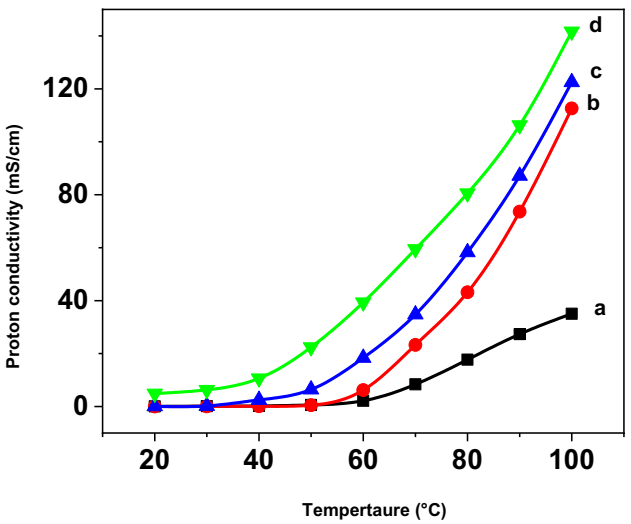

Fig. 7 Evaluation of proton conductivity of **a** LSPSO, **b** 1 wt% Hect/LSPSO, **c** 3 wt% Hect/LSPSO and **d** 6 wt% Hect/LSPSO at 100% relative Humidity

membranes we prepared exhibit higher proton conductivity values compared to those of the commercially available Nafion®117 membrane, measured under the same experimental conditions [26]. The relationship between temperature and proton conductivity can be elucidated by employing the Arrhenius equation, which provides a method for calculating the activation energy linked to conductivity. The formula for determining this activation energy is expressed as Eq. 5:

$$\sigma = \sigma_0 \exp(-E_a/RT). \quad (5)$$

This equation facilitates the quantification of the activation energy linked to proton conductivity, drawing upon the temperature-dependent characteristics observed in the study. In this context, σ signifies proton conductivity in Siemens per centimeter (S/cm), σ_0 represents the preexponential factor, R corresponds to the universal gas constant, which has a constant value of 8.314472 J/mol·K, and T indicates the absolute temperature, measured in Kelvin (K). Table 3 in the research document presents activation energies for both LSPSO and the corresponding nanocomposite layers.

The determination of these activation energies was carried out through the utilization of Eq. 5 and the data were derived from experiments conducted under a controlled condition of 100% relative humidity (RH). Table 3 serves as a comprehensive compilation, summarizing the activation energies for both the LSPSO membrane and its corresponding nanocomposite counterparts, thereby providing valuable insights into their conductivity characteristics. This assessment of activation energy was performed for both the composite and LSPSO membranes within an experimental framework featuring a consistent 100% relative humidity (RH). The outcomes laid out in Table 3 unambiguously highlight that the composite membranes manifest notably reduced activation energy values when juxtaposed with their counterparts composed solely of unaltered LSPSO. The inclusion of the filler material exerts a pronounced impact on the activation energy, with the composite membrane incorporating 6 wt% clay registering the most diminished value. This discovery reinforces the prior observations, solidifying the assertion that the composite membranes indeed exhibit enhanced proton conductivity.

Table 3 Activation energy values and proton conductivity at 100 °C

Membrane	Conductivity (mS/cm) at 100 °C	E_a (kJ/mol)
LSPSO	35.04	100
1 wt% Hect/LSPSO	112.61	71
3 wt% Hect/LSPSO	122.52	70
6 wt% Hect/LSPSO	141.66	68

Conclusion and future outlook

The production of composite membranes involved using low-sulfonated polyether sulfone octyl sulfonamide (LSPSO) with a sulfonation level of 0.9 per monomer unit (pmu) as the base material and integrating different amounts of Hectorite clay.

Our investigation revealed a strong association between the clay concentration within the membrane and its characteristics, including contact angle, ion exchange capacity, moisture absorption, and proton conductivity. Incorporating Hectorite clay resulted in several notable effects on the membrane's properties. Importantly, it led to significant improvements in water absorption, ion exchange capacity (IEC), scanning electron microscopy (SEM) features, and contact angle measurements. Furthermore, it significantly bolstered the effectiveness of protonic conduction when contrasted with pristine low sulfonated polyether sulfone octyl sulfonamide (LSPSO). The most favorable composite, composed of 6 wt% Hectorite (Hect) in conjunction with LSPSO, showcased protonic conductivity values that were fourfold higher than those observed in pure LSPSO when subjected to high-temperature and high-humidity conditions. These membranes show substantial promise in various applications, including proton exchange membrane fuel cells, reverse osmosis, ultrafiltration, electrode production (using laser-induced graphene), and the development of supercapacitors through laser writing on membrane films, among other potential uses.

Supplementary Information The online version contains supplementary material available at https://doi.org/10.1007/s40243-023-00251-6.

Acknowledgements The authors extend their appreciation to the manager of Eras Labo Fabrice MORELLE, and his employers Serge VIDAL et Lionel Ogier (Saint-Nazaire-Les-Eymes, France) for generously supplying the Low Sulfonated Polyether Sulfone Octyl Sulfonamide (LSPSO) polymer at no cost.

Author contributions WM: formal analysis, investigation, methodology, writing original draft, writing—review and editing; KC: data curation, measurements, formal analysis, investigation, writing—original draft; IBK: investigation, measurements, resources, data curation, formal analysis, visualization; NB: visualization, measurements, resources; RM: data curation, investigation, funding acquisition, writing original draft; SMASK: conceptualization, investigation. Writing review and editing, visualization, supervision, funding acquisition. All authors gave final approval for publication and agreed to be held accountable for the work performed therein.

Declarations

Conflict of interest The authors declare that they have no conflict of interest.

References

1. Chen, G., Zhang, H., Cheng, J., Ma, Y., Zhong, H.: A novel membrane electrode assembly for improving the efficiency of the unitized regenerative fuel cell. Electrochem. Commun.. Commun. **10**, 1373–1376 (2008). https://doi.org/10.1016/j.elecom.2008.07.002
2. Mabrouk, W., Charradi, K., Lafi, R., AlSalem, H.S., Maghraoui-Meherzi, H., Keshk, S.M.A.S.: Augmentation in proton conductivity of sulfonated polyether sulfone octyl sulfonamide using sepiolite clay. J. Mater. Sci. **57**, 15331–15339 (2022). https://doi.org/10.1007/s10853-022-07627-5
3. Mabrouk, W., Lafi, R., Fauvarque, J.F., Hafiane, A., Sollogoub, C.: New ion exchange membrane derived from sulfochlorated polyether sulfone for electrodialysis desalination of brackish water. Polym. Adv. Technol.. Adv. Technol. **32**, 304–314 (2021). https://doi.org/10.1002/pat.5086
4. Baachaoui, S., Mabrouk, W., Charradi, K., Slimi, B., Ramadan, A.M., Elsamra, R.M.I., Keshk, S.M.A.S., Raouafi, N.: Laser-induced porous graphene electrodes from polyketmine membranes for Paracetamol sensing. R. Soc. Open. Sci. **10**, 230294 (2023). https://doi.org/10.1098/rsos.230294
5. Baachaoui, S., Mabrouk, W., Rabti, A., Ghodbane, O., Raouafi, N.: Laser-induced graphene electrodes scribed onto novel carbon black-doped polyethersulfone for flexible high-performance. J. Colloid. Interf. Sci. **646**, 1–10 (2023). https://doi.org/10.1016/j.jcis.2023.05.024
6. Vinodh, R., Atchudan, R., Kim, H.J., Yi, M.: Recent advancements in polysulfone based membranes for fuel cell (PEMFCs, DMFCs, and AMFCs) applications: a critical review. Polymers **14**, 300 (2022). https://doi.org/10.3390/polym14020300
7. Maier, G., Meier-Haack, J.: Sulfonated aromatic polymers for fuel cell membranes. Adv. Polym. Sci.Polym. Sci. **216**, 1–62 (2008). https://doi.org/10.1007/12_2008_135
8. Mabrouk, W., Ogier, L., Vidal, S., Sollogoub, C., Matoussi, F., Dachraoui, M., et al.: Synthesis and characterization of polymer blends of sulfonated polyethersulfone and sulfonated polyethersulfone octylsulfonamide for PEMFC applications. Fuel Cells. **2**, 179–187 (2012). https://doi.org/10.1002/fuce.201100051
9. Ahmed, Z., Charradi, K., Alsulami, Q.A., Keshk, S.M.A.S., Chtourou, R.: Physicochemical characterization of low sulfonated polyether ether ketone/Smectite clay composite for proton exchange membrane fuel cells. J. Appl. Polym. Sci.Polym. Sci. **138**, 49634–49642 (2021). https://doi.org/10.1002/app.49634
10. Mabrouk, W., Ogier, L., Matoussi, F., Sollogoub, C., Vidal, S., Dachraoui, M., et al.: Preparation of new proton exchange membranes using sulfonated poly(ethersulfone) modified by octylamine (SPESOS). Mater. Chem. Phys. **28**, 456–463 (2011). https://doi.org/10.1016/j.matchemphys.2011.03.031
11. Simari, C., Lo Vecchio, C., Baglio, V., Nicotera, I.: Sulfonated polyethersulfone/poly ether ether ketone blend as high performing and cost-effective electrolyte membrane for direct methanol fuel cells. Renew. Energy Energy **159**, 336–345 (2020). https://doi.org/10.1016/j.renene.2020.06.053
12. Mabrouk, W., Charradi, K., Maghraoui-Meherzi, H., Alhussein, H.A., Keshk, S.M.A.S.: Proton conductivity amelioration of sulfonated poly ether sulfone octyl sulfonamide via the incorporation of montmorillonite. J. Electron. Mater. **51**, 6369–6378 (2022). https://doi.org/10.1007/s11664-022-09862-7
13. Mabrouk, W., Charradi, K., Mellekh, A., Hafiane, A., Alsulami, Q.A., Maghraoui-Meherzi, H., et al.: Enhanced proton conductivity of a sulfonated polyether sulfone octyl sulfonamide membrane via the incorporation of protonated montmorillonite. J. Electron. Mater. **52**, 2158–2167 (2023). https://doi.org/10.1007/s11664-022-10183-y
14. Zhang, J., Zhou, C.H., Petit, S., Zhang, H.: Hectorite: synthesis, modification, assembly and applications. Appl. Clay Sci. **177**, 114–138 (2019). https://doi.org/10.1016/j.clay.2019.05.001
15. Mabrouk, W., Jebri, S., Charradi, K., Slimi, B., Alzahrani, A.Y.A., Boubakri, A., et al.: Fabrication and characterization of graphene/sulfonated polyether sulfone octyl sulfonamide hybrid film with improved proton conductivity performance. J. Solid. State. Electr. **27**, 991–999 (2023). https://doi.org/10.1007/s10008-023-05411-2
16. Mabrouk, W., Ogier, L., Vidal, S., Sollogoub, C., Matoussi, F., Fauvarque, J.F.: Ion exchange membranes based upon crosslinked sulfonated polyethersulfone for electrochemical applications. J. Membrane Sci. **452**, 363–270 (2014). https://doi.org/10.1016/j.memsci.2013.10.006
17. Mabrouk, W., Ogier, L., Sollogoub, C., Vidal, S., Matoussi, F., Fauvarque, J.F.: Synthesis and characterization of new membranes deriving from sulfonated polyethersulfone for PEMFC applications. Desalin. Water Treat. **56**, 2637–2645 (2015). https://doi.org/10.1080/19443994.2015.1024939
18. Thmaini, N., Charradi, K., Ahmed, Z., Chtourou, R., Aranda, P.: Nanoarchitectonics of fibrous clays as fillers of improved proton-conducting membranes for fuel-cell applications. Appl. Clay Sci. **242**, 107019 (2023). https://doi.org/10.1016/j.clay.2023.107019
19. Mabrouk, W., Lafi, R., Charradi, K., Ogier, L., Hafiane, A., Fauvarque, J.F., et al.: Synthesis and characterization of new proton exchange membrane deriving from sulfonated polyether sulfone using ionic crosslinking for electrodialysis applications. Polym. Eng. Sci. **60**, 3149–3158 (2020). https://doi.org/10.1002/pen.25543
20. Mabrouk, W., Lafi, R., Hafiane, A.: Electrodialysis performance during the defluoridation of brackish water using ClNH2 membrane. Desalin. Water Treat. **236**, 16–25 (2021). https://doi.org/10.5004/dwt.2021.27669
21. Thangamuthu, P., Moothy, S., Mahimia, B.M., Kannaiyan, D., Deivanayagam, P.: High performance bismuth oxide embedded sulfonated poly ether sulfone composite membranes for fuel cell applications. J. Macromol. Sci. A. **60**, 171–180 (2023). https://doi.org/10.1080/10601325.2023.2186793
22. Charradi, K., Landolsi, Z., Gabriel, L., Mabrouk, W., Koschella, A., Ahmed, Z., et al.: Incorporation of sulfo ethyl cellulose tp augment the performance of sulfonated poly (ether ether ketone) composite for proton exchange membrane fuel cells. J. Solid. State. Electr. **27**, 991–999 (2023). https://doi.org/10.1007/s10008-023-05629-0
23. Eskitoros-Togay, S.M., Emre Bulbul, Y., Cınar, Z.K., Sahin, A., Dilsiz, N.: Fabrication of PVP/sulfonated PES electrospun membranes decorated by sulfonated halloysite nanotubes via electrospinning method and enhanced performance of proton exchange

membrane fuel cells. Int. J. Hydrogen. Energ. **48**, 280–290 (2023). https://doi.org/10.1016/j.ijhydene.2022.09.214
24. Charradi, K., Chemek, M., Slimi, B., Ramadan, A.M., Alzahrani, A.Y.A., Chtourou, R., et al.: Fabrication and characterization of polyvalent metals/oxidized polyvinyl alcohol hybrid films with improved proton conductivity and optical performances. J. Polym. Environ. **31**, 3167–3181 (2023). https://doi.org/10.1007/s10924-023-02824-y
25. Bagryantseva, I.N., Ponomareva, V.G., Khusnutdinov, V.R.: Intermediate temperature proton electrolytes based on cesium dihydrogen phosphate and poly(vinylidene fluoride-co-hexafluoropropylene. J. Mater. Sci. **56**, 14196–14206 (2021). https://doi.org/10.1007/s10853-021-06137-0
26. Charradi, K., Ahmed, Z., Cid, R.E., Aranda, P., Ruiz-Hitzky, E., Ocon, P., Chtourou, R.: Amelioration of PEMFC performance at high temperature by incorporation of nanofiller (sepiolite/layered double hydroxide) in Nafion membrane. Int. J. Hydrogen. Energ. **44**, 10666–10676 (2019). https://doi.org/10.1016/j.ijhydene.2019.02.183